ABC UTC
ACCELERATED BRIDGE CONSTRUCTION
UNIVERSITY TRANSPORTATION CENTER

ABC-UTC GUIDE FOR:

ASSESSING THE EFFECTS OF FREQUENT, LOW-LEVEL SEISMIC EVENTS

January 2020

End Date:

July 30, 2019

Performing Institution:

University of Oklahoma

Name of PIs:

P. S. Harvey Jr., Ph.D., P.E. &
K. K. Muraleetharan, Ph.D., P.E., G.E.

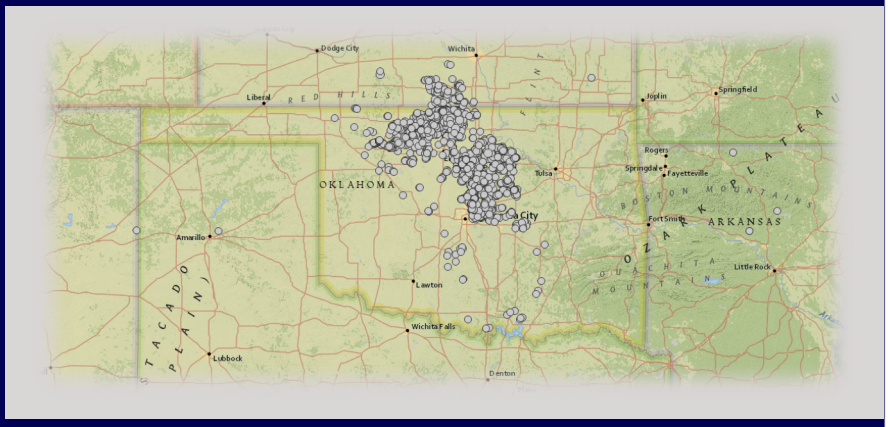

IOWA STATE UNIVERSITY

University of Nevada, Reno

FIU
Civil and Environmental Engineering

WASHINGTON

The UNIVERSITY of OKLAHOMA

TABLE OF CONTENTS

ABSTRACT

States such as Oklahoma, Texas, Kansas and Arkansas have historically experienced only one or two tectonic earthquakes annually, but these states are now experiencing earthquakes at an increased rate due to induced seismicity. Consequently, State Departments of Transportation (DOTs) are concerned about how their bridges that were originally designed for low seismic design loads will handle this increased seismic demand. While a bridge collapse is unlikely for an induced earthquake, cumulative effects of large number of small induced earthquakes compounded with an occasional moderate earthquake may lead to damages negatively impacting the safety of the traveling public and the flow of the transportation network. This document provides a practical guide that bridge owners and consultants can use to assess the cumulative effect of a large number of small-to-moderate earthquakes on a bridge. A new metric called the *fatigue damage index* (FDI) is proposed, which can be used to capture structural deterioration due to accumulated seismic damage. This guide details the appropriate use of the FDI framework developed through this research project to quantify how close a bridge is to its fatigue limit for a given earthquake sequence, from which the remaining service life can be determined. The FDI can also be used to predict when accelerated repairs may be required and to evaluate accelerated retrofit solutions.

ACKNOWLEDGEMENTS

This project was supported by the Accelerated Bridge Construction University Transportation Center (ABC-UTC at www.abc-utc.fiu.edu) at Florida International University (FIU) as lead institution and Iowa State University (ISU), the University of Nevada-Reno (UNR), the University of Oklahoma (OU), and the University of Washington (UW) as partner institutions. The authors would like to acknowledge the ABC-UTC support.

The authors would like to extend special appreciation to the ABC-UTC and the U.S. Department of Transportation Office of the Assistant Secretary for Research and Technology for funding this project.

The authors would like to also thank the project Research Advisory Panel members: Walter Peters and Steve Jacobi from Oklahoma DOT and Gregg Hostetler from CONSOR Engineers (formerly Infrastructure Engineers).

1 — INTRODUCTION

1.1 — BACKGROUND

Since 2009, there has been a dramatic increase in the number of earthquakes in the central U.S. (Figure 1.1). States such as Oklahoma, Texas, Kansas, and Arkansas have not historically experienced earthquakes at the rate currently observed, nor of this magnitude (McGarr et al., 2015). Studies have linked the increased rate of seismic activity since 2009 to wastewater injection in disposal wells (Keranen et al., 2013). The seismicity of places such as California and the New Madrid seismic zone is well documented and generally thought of when discussing seismic hazards in the contiguous U.S. Yet the cumulative moment in Oklahoma in 2015 and 2016 (1 January 2015 to 31 December 2016) exceeded that of southern California and the New Madrid seismic zones.

The major fault in the central U.S. is the New Madrid fault (Frankel et al., 2009) located along the Mississippi River between Tennessee, Arkansas, Missouri, and Kentucky. The only other identified source of tectonic earthquakes in this region is the Meer's fault in southwest Oklahoma, as reflected in the U.S. Geological Survey (USGS) national seismic hazard maps (Petersen et al., 2014) and accordingly the mapped design ground motion data provided by design provisions, such as the *2009 AASHTO Guide Specifications for LRFD Seismic Bridge Design* (AASHTO, 2009). In 2016, the USGS made an effort to incorporate non-tectonic earthquakes (or "induced seismicity") into the national seismic hazard model (Petersen et al., 2016), but these are not reflected in seismic design provisions. Accordingly, concern has risen about how civil infrastructure in the central U.S. will handle the increased seismic demand (Harvey et al., 2018a).

A majority of the earthquakes occurring in the central U.S. are small-to-moderate in magnitude, ranging from magnitude (M) 3.0 to 5.0. Over the last decade, the central U.S. has experienced nearly 120 M4.0 and greater earthquakes, with a majority (81) occurring in Oklahoma. While collapse is unlikely for the induced earthquakes currently observed (Harvey et al., 2018b; Chase et al., 2019), the cumulative effects of a large number of small-to-moderate earthquakes on bridges are not fully understood. These cumulative effects compounded with the occasional moderate earthquake (M5.0 and larger) may lead to damage requiring rapid repairs to avoid acute traffic control issues at the affected bridge sites. To reduce impacts to the driving public, *accelerated bridge construction* (ABC) techniques

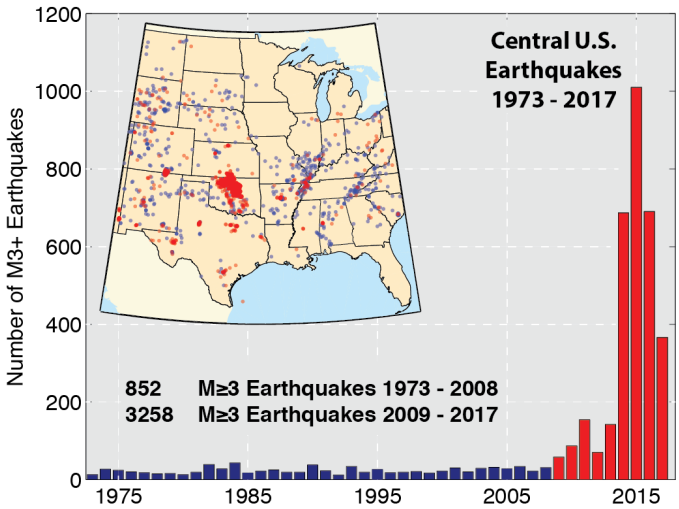

Figure 1.1: Cumulative number of earthquakes with a magnitude 3.0 or larger in the central United States (USGS, 2017).

have been developed over recent years (Culmo, 2011), but have primarily focused on rapidly constructing new or replacement structures. Another benefit derived from these ABC methods is rapid post-earthquake repair of damaged structures, for example accelerated column repair/replacement with carbon fiber wrapping and steel casings. This research addressed the existing knowledge gap on assessing the effects of frequent, low-level seismic events on bridges with the aim of determining when/where accelerated repairs may be needed.

1.2 — PROBLEM STATEMENT

The recent surge in seismic activity in the central U.S. has motivated the need for rapid repair techniques that leverage ABC methods. The overarching objective of this research was to develop analysis techniques to study the effect of large number of small-to-moderate earthquakes on bridges. The project considered Oklahoma as a case study and developed techniques and tools that can be applied to other regions experiencing low-level frequent seismic events. Ultimately, the research resulted in the following outcomes:

(a) new seismic analysis tools to assess for damage from repeated, small-to-moderate earthquakes;

(b) a guide for the appropriate use of these tools.

1.3 — SCOPE OF THE GUIDE

The objective of this document is to provide a practical ABC-UTC guide with which bridge owners and consultants can assess the cumulative effect of a large number of small-to-moderate earthquakes. The proposed *fatigue damage index* (FDI) can be used to capture structural deterioration due to accumulated seismic damage by quantifying how close a bridge is to its fatigue limit for a given earthquake sequence, from which the remaining service life can be determined. This ABC-UTC guide details the appropriate use of the FDI framework developed through this research project. The final report for this research project (Harvey et al., 2020) provides additional details on the FDI framework, as well as a working example.

2 — BACKGROUND CONCEPTS

2.1 — FATIGUE ANALYSIS

Fatigue is the weakening of a material caused by repeated applied loads. Fatigue occurs at stress values much less than the yield or ultimate strength of the material. Material performance is commonly characterized by an S–N curve, which represents the number of cycles to failure, N, for a given magnitude of cyclic stress, S. These curves assume repeated cycles at the same cyclic stress magnitude. This assumption is not valid when considering bridges subjected to repeated seismic loads. That is, the amplitude of cycles will vary considerably during a single event, as well as under different events of different magnitude located at different distances from the bridge. Therefore, a spectrum of stress magnitudes, S_k $(k = 1, 2, \ldots, K)$, is expected, each contributing n_k cycles. Each of these stress magnitudes has a corresponding number of cycles to failure, $N_k(S_k)$. The most popular method to account for the spectrum of stresses and number of cycles is *Miner's Rule* (Miner, 1945):

$$C = \sum_{k=1}^{K} \frac{n_k}{N_k} \tag{2.1.1}$$

where the material will fail in fatigue when the damage fraction, C, equals 1. The interpretation of Miner's rule is that the fractions of the life consumed at each stress level, n_k/N_k ($k = 1, 2, \ldots, K$), linearly combine with one another. Note that Miner's rule does not take into account the order in which the cyclic loads are applied.

An approach based on Miner's rule is assumed in this work. This requires counting the number of cycles a bridge is subjected to when excited by a sequence of earthquakes. The standard practice for cycle counting in fatigue analysis is *rainflow counting* (ASTM E1049-85(2017), 2017), originally proposed by Matsuishi and Endo (1968). Rainflow counting will be used to quantify the cyclic demand on bridges and is briefly described here.

2.2 — RAINFLOW COUNTING

Fatigue cycles are the repeated loading and unloading of an object that accumulates damage in its material. Cycles can be counted on time histories of force, stress, strain, torque, acceleration, deflection, or other loading parameters of interest. One of the most widely used cycle counting algorithms is rainflow counting, which was included as one of the cycle counting algorithms in ASTM E1049-85(2017) (2017). Since Matsuishi and Endo (1968) initially proposed the rainflow counting algorithm, different types of fatigue cycle counting methods such as level-crossing counting, peak counting, simple-range counting, and simplified rainflow counting have been introduced to summarize random or transient load time histories by providing the number of cycles at various ranges (ASTM E1049-85(2017), 2017). The counting algorithm, definitions of cyclic parameters, and the results vary with the type of counting method used. For this work, the rainflow counting algorithm per ASTM standards was utilized.

The `rainflow` function in Matlab (Mathworks, Natick, MA) is based on the ASTM standard. A load time history with a sequence of reversals is input into `rainflow`. Reversals are the local minima and maxima where the first derivative of load time history changes its sign. This `rainflow` function counts cycles by tracking a moving three-point subset of points and a moving reference point (say Point Z) explained as follows:

1. The first and second point in the subset are grouped together and are denoted Y.
2. The second and third point in the subset are grouped together and are denoted X.
3. In groups X and Y, the points are sorted from earlier to later in time but are not necessarily consecutive points in the load time history.
4. The range of X, denoted $r(X)$, is the absolute value of the difference between the amplitude of the first point and the amplitude of the second point, and $r(Y)$ is the absolute value of the difference between the amplitude of the second point and the amplitude of the third point.

Figure 2.1 depicts the rainflow counting algorithm. At the end, the rainflow function collects the different cycles and half-cycles and tabulates their ranges (peak to valley), their means, and the points at which they start and end. This algorithm is recommended for cycle counting in the FDI framework, described in the following section.

3 — FATIGUE DAMAGE INDEX (FDI) FRAMEWORK

The proposed framework aims to evaluate the potential for cumulative damage (high-cycle fatigue) in structures caused by many small-to-moderate induced earthquakes. To this end, the framework characterizes the cumulative cyclic demand on a bridge for a desired set of ground motion data and compares the demand against the capacity of a structural member to assess the likelihood of fatigue.

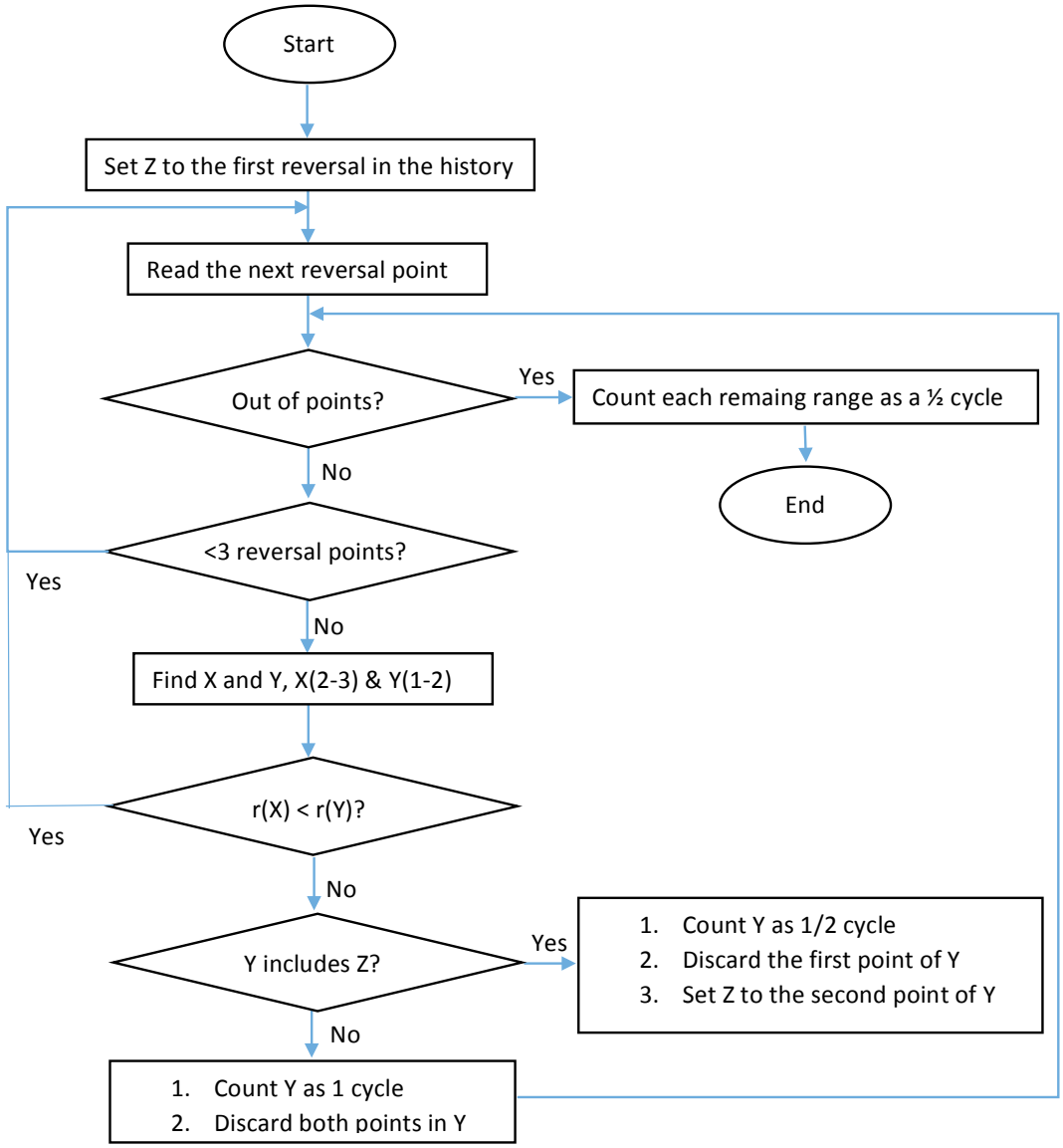

Figure 2.1: Rainflow counting algorithm.

A new metric, the *fatigue damage index* (FDI), is used to quantify the proportion of the fatigue life that is accumulated and can estimate the remaining service life of the structure. The FDI framework is illustrated in Figure 3.1 and is comprised of five steps described here.

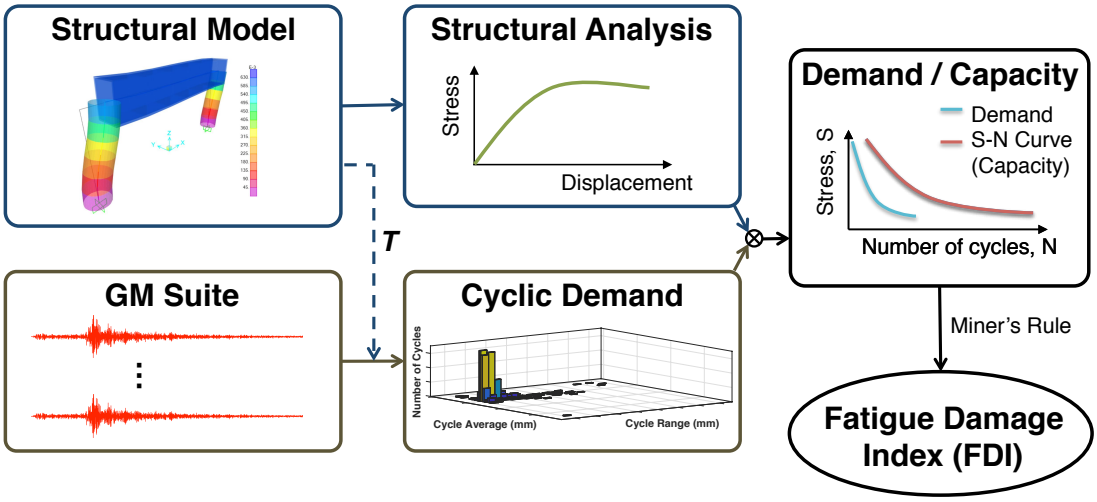

Figure 3.1: Fatigue damage index (FDI) framework.

3.1 — STEP 1 – MATHEMATICAL MODEL OF THE IMPACTED BRIDGE

The first step of the FDI framework is to develop a mathematical model of the impacted bridge of interest—either a "typical" bridge or a specific bridge. This model is used to determine the natural modes of vibration for the bridge. Assuming that the bridge has two axes of symmetry subjected to bidirectional horizontal GM along these axes, then the modal responses in the orthogonal directions—longitudinal (x) and transverse (y)—can be treated independently. Furthermore, it is initially assumed that a single (fundamental) mode in each of the orthogonal directions of response is sufficient.

The fundamental modes of vibration can be determined by either some approximate method or modal analysis. To this end, the model may be quite simple or very detailed, depending on the application. For example, the former might assume a single-degree-of-freedom (SDOF) model for the structure in each direction, e.g.,

$$\tilde{m}_x\ddot{x}(t) + \tilde{c}_x\dot{x}(t) + \tilde{k}_x x(t) = -\tilde{m}_x\tilde{\Gamma}_x\ddot{x}_g(t) \tag{3.1.1a}$$

$$\tilde{m}_y\ddot{y}(t) + \tilde{c}_y\dot{y}(t) + \tilde{k}_y y(t) = -\tilde{m}_y\tilde{\Gamma}_y\ddot{y}_g(t) \tag{3.1.1b}$$

whereas the latter might involve a fully nonlinear three-dimensional finite element (FE) model to represent the structure, e.g.,

$$\mathbf{M}\ddot{\mathbf{q}}(t) + \mathbf{C}\dot{\mathbf{q}}(t) + \mathbf{f}(\mathbf{q}(t)) = -\mathbf{M}\boldsymbol{\iota}_x\ddot{x}_g(t) - \mathbf{M}\boldsymbol{\iota}_y\ddot{y}_g(t) \tag{3.1.2}$$

where $\ddot{x}_g(t)$ and $\ddot{y}_g(t)$ are the orthogonal horizontal GMs. In Eq. (3.1.1), $x(t)$ and $y(t)$ are the generalized displacements in orthogonal directions (longitudinal and transverse, respectively), with associated generalized mass $\tilde{m}$, damping $\tilde{c}$, stiffness $\tilde{k}$, and mode participation factor $\tilde{\Gamma}$.* In Eq. (3.1.2), $\mathbf{q}(t)$ is the vector of generalized coordinates, $\mathbf{M}$ and $\mathbf{C}$ are the mass and damping matrices, $\mathbf{f}(\cdot)$ is the nonlinear

*Following the notation of Chopra (2017).

restoring force, and $\boldsymbol{\iota}_x$ and $\boldsymbol{\iota}_y$ are the influence vectors for $\ddot{x}_g(t)$ and $\ddot{y}_g(t)$, respectively. Eq. (3.1.2) can be linearized as follows:

$$\mathbf{M}\ddot{\mathbf{q}}(t) + \mathbf{C}\dot{\mathbf{q}}(t) + \mathbf{K}\mathbf{q}(t) = -\mathbf{M}\boldsymbol{\iota}_x\ddot{x}_g(t) - \mathbf{M}\boldsymbol{\iota}_y\ddot{y}_g(t), \tag{3.1.3}$$

where $\mathbf{K}$ is the stiffness matrix. Under the assumption of plan symmetry about both x and y axes, the responses in the orthogonal directions can be treated independently:

$$\mathbf{M}_x\ddot{\mathbf{q}}_x(t) + \mathbf{C}_x\dot{\mathbf{q}}_x(t) + \mathbf{K}_x\mathbf{q}_x(t) = -\mathbf{M}_x\boldsymbol{\iota}_x\ddot{x}_g(t), \tag{3.1.4a}$$

$$\mathbf{M}_y\ddot{\mathbf{q}}_y(t) + \mathbf{C}_y\dot{\mathbf{q}}_y(t) + \mathbf{K}_y\mathbf{q}_y(t) = -\mathbf{M}_y\boldsymbol{\iota}_y\ddot{y}_g(t), \tag{3.1.4b}$$

where the subscripts x and y are used to distinguish the response in the orthogonal directions.

For the simple model given by Eq. (3.1.1), the modal properties are found immediately:

$$\omega_x = \left(\tilde{k}_x/\tilde{m}_x\right)^{1/2} \quad \text{and} \quad \omega_y = \left(\tilde{k}_y/\tilde{m}_y\right)^{1/2} \tag{3.1.5}$$

Generally, the damping coefficients $\tilde{c}_x$ and $\tilde{c}_y$ are not determined directly, but instead values for the modal damping ratios ζ_x and ζ_y are assumed. For the linearized FE model given by Eq. (3.1.4), the lowest J natural frequencies (ω_{xj} and ω_{yj}, $j = 1, \ldots, J$) and associated mode shapes ($\boldsymbol{\phi}_{xj}$ and $\boldsymbol{\phi}_{yj}$) of the structure are found by solving the eigenvalue problem, $(\mathbf{K}_\xi - \omega^2\mathbf{M}_\xi)\boldsymbol{\phi} = \mathbf{0}$ for $\xi = x, y$. Modal damping ratios (ζ_{xj} and ζ_{yj}) are generally assumed or found from classical damping estimates (e.g., Rayleigh damping).

3.2 — STEP 2 – COMPILE GROUND-MOTION DATA

The next step is to compile and organize a sequence of ground motions (GMs) impacting the bridge during the time frame of interest (e.g., one calendar year) and in the desired range of earthquake magnitudes (e.g., greater than some magnitude threshold). The GM sequence is composed of N bidirectional horizontal GMs, here denoted:

$$\mathcal{S} = \left\{\left(a_{NS}^{(i)}(t), a_{EW}^{(i)}(t)\right) : i = 1, \ldots, N\right\} \tag{3.2.1}$$

where $a_{NS}(t)$ and $a_{EW}(t)$ are the ground accelerations in the north-south and east-west directions, respectively. Because GM measurements are taken at seismic stations that are most likely not colocated with the structure of interest, seismic stations should be selected to be roughly representative of the seismic hazard at the structure's actual site.

3.3 — STEP 3 – CHARACTERIZE THE CYCLIC SEISMIC DEMAND

To quantify the cyclic seismic demand, simple harmonic oscillators representative of the structure are subjected to the sequence $\mathcal{S}$ of earthquake ground motions acquired in Step 2. For each oscillator, the displacement response is computed independently for the two components of horizontal GM:

$$\ddot{D}_{NS}^{(i)}(t) + 2\zeta\omega\dot{D}_{NS}^{(i)}(t) + \omega^2 D_{NS}^{(i)}(t) = -a_{NS}^{(i)}(t) \tag{3.3.1a}$$

$$\ddot{D}_{EW}^{(i)}(t) + 2\zeta\omega\dot{D}_{EW}^{(i)}(t) + \omega^2 D_{EW}^{(i)}(t) = -a_{EW}^{(i)}(t) \tag{3.3.1b}$$

for $i = 1, \ldots, N$. The properties of the SDOF oscillators (i.e., natural frequencies $\omega = 2\pi/T$ and damping ratios ζ) are based upon the modal properties of the structure found in Step 1. For now, the subscripts "x" and "y" are dropped for brevity. The notation $D_{NS}^{(i)}(t \,|\, \omega, \zeta)$ and $D_{EW}^{(i)}(t \,|\, \omega, \zeta)$ will be used hereinafter

to denote the displacement response time history of an SDOF oscillator, with properties ω and ζ, in the NS and EW directions, respectively, due to the ith GM. The cyclic seismic demand is characterized by the displacement cycle ranges and counts based on these simple oscillators, which will be related to physical displacements (and stresses) in the structure in Step 4.

As discussed in Section 2.2, there are many different cycle-counting methods available for use (ASTM E1049-85(2017), 2017). Here, displacement cycles are counted using rainflow counting (Matsuishi and Endo, 1968). Rainflow counting is performed independently for each displacement time history, i.e., for each GM ($i = 1, \ldots, N$) in each orthogonal direction (NS and EW). For each case, the rainflow counting algorithm returns a set of displacement cycle ranges $\overline{D}$ with associated cycle counts (1 or 1/2).[†] The displacement cycle ranges are then distributed among K displacement bins

$$\mathcal{D}_k = \left\{ \overline{D} : \overline{D}_{k-1} < \overline{D} \leqslant \overline{D}_k \right\}, \; k = 1, 2, \ldots, K \tag{3.3.2}$$

where $\overline{D}_0 = 0$, and the cycle counts are summed within each bin. The summed displacement cycle counts in bin $\mathcal{D}_k$ are denoted $n^{(i)}_{D_{NS}}(\overline{D}_k \,|\, \omega, \zeta)$ and $n^{(i)}_{D_{EW}}(\overline{D}_k \,|\, \omega, \zeta)$, which are characterized by the upper bin edge $\overline{D}_k$. The same bins are used for all GMs ($i = 1, \ldots, N$), and their counts are combined:

$$n_{D_{NS}}(\overline{D}_k \,|\, \omega, \zeta) = \sum_{i=1}^{N} n^{(i)}_{D_{NS}}(\overline{D}_k \,|\, \omega, \zeta) \;\text{ and }\; n_{D_{EW}}(\overline{D}_k \,|\, \omega, \zeta) = \sum_{i=1}^{N} n^{(i)}_{D_{EW}}(\overline{D}_k \,|\, \omega, \zeta) \tag{3.3.3}$$

Finally, for each bin, the cycle counts in orthogonal directions are combined by taking the square root of the sum of the squares (SRSS):

$$n_D(\overline{D}_k \,|\, \omega, \zeta) = \sqrt{[n_{D_{NS}}(\overline{D}_k \,|\, \omega, \zeta)]^2 + [n_{D_{EW}}(\overline{D}_k \,|\, \omega, \zeta)]^2} \tag{3.3.4}$$

for $k = 1, \ldots, K$. Combining the EW and NS counts in this manner accounts for uncertainty in the orientation of the structure with respect to the cardinal directions, which is analogous to using the geometric mean of spectral ordinates for uniaxial design spectral accelerations (Beyer and Bommer, 2006; Boore et al., 2006). The displacement cycle ranges $\overline{D}_k$ found in this step are representative of *spectral displacements*, and they are mapped to stress cycle ranges in the next step. The combination of the modal responses is treated in Step 5.

3.4 — STEP 4 – STRUCTURAL ANALYSIS

In this step, the spectral response displacement ranges $\overline{D}_k$ are related to stresses within the structure. First, consider the simple SDOF structural models given in Eq. (3.1.1). In this case, the spectral displacement D is related to the generalized displacements x and y through the mode participation factor, i.e., $x = \tilde{\Gamma}_x D$ and $y = \tilde{\Gamma}_y D$. The spectral displacement ranges $\overline{D}_k$ are mapped to stress ranges $\overline{s}_{xk}$ and $\overline{s}_{yk}$ of a particular location within the structure (e.g., a weld). To do so, apply equivalent static lateral loads

$$\tilde{P}_{xk} = \tilde{m}_x \tilde{\Gamma}_x \omega_x^2 \frac{\overline{D}_k}{2} \quad \text{and} \quad \tilde{P}_{yk} = \tilde{m}_y \tilde{\Gamma}_y \omega_y^2 \frac{\overline{D}_k}{2} \tag{3.4.1}$$

to the structure,[‡] and determine the resulting stresses s_{xk} and s_{yk}, respectively. The stress ranges are taken to be

$$\overline{s}_{xk} = 2 \times s_{xk} \quad \text{and} \quad \overline{s}_{yk} = 2 \times s_{yk} \tag{3.4.2}$$

[†]Here, an over line ($\overline{\cdot}$) is used to represent a cycle *range* (peak to valley), which is to be distinguished from a cycle amplitude taken to be half the range.

[‡]Note that the $1/2$ appearing in Eq. (3.4.1) is to consider the load *amplitude*, taken to be half of the load range.

with corresponding stress cycle counts $n_s(\overline{s}_{xk}) \equiv n_D(\overline{D}_k \,|\, \omega_x, \zeta_x)$ and $n_s(\overline{s}_{yk}) \equiv n_D(\overline{D}_k \,|\, \omega_y, \zeta_y)$. Note that $\overline{s}_{xk} \neq \overline{s}_{yk}$ in general.

Next, consider the linearized FE models given in Eq. (3.1.4). As in a response spectrum analysis, stresses within elements of the structure are found by applying equivalent static loads $\mathbf{P}_{\xi j}$ ($\xi = x, y$) to the structure. These loads are given by

$$\mathbf{P}_{\xi j}(D) = \Gamma_{\xi j}\mathbf{M}_\xi \boldsymbol{\phi}_{\xi j}\omega_{\xi j}^2 D \;\text{ where }\; \Gamma_{\xi j} = \frac{\boldsymbol{\phi}_{\xi j}^T \mathbf{M}_\xi \boldsymbol{\iota}_\xi}{\boldsymbol{\phi}_{\xi j}^T \mathbf{M}_\xi \boldsymbol{\phi}_{\xi j}} \tag{3.4.3}$$

Applying these static loads to the structure at spectral displacements amplitude $D = \overline{D}_1/2, \ldots, \overline{D}_K/2$, the corresponding stress amplitudes (denoted $s_1, \ldots, s_K$) are found. Letting $s_{\xi jk}$ denote the kth stress amplitude in the jth mode ($j = 1, \ldots, J$) in the ξ direction ($\xi = x, y$), the stress cycle counts are then given by $n_s(\overline{s}_{\xi jk}) \equiv n_D(\overline{D}_k \,|\, \omega_{\xi j}, \zeta_{\xi j})$ where $\overline{s}_{\xi jk} = 2 \times s_{\xi jk}$.

3.5 — STEP 5 – DEMAND/CAPACITY ANALYSIS

In this step, the demand on and capacity of the structure are combined with one another to determine the potential for fatigue. The demand is characterized by the stress cycle counts and ranges determined in Step 4. The capacity of the particular structural element of interest is characterized by the material's S–N curve. An S–N curve represents number of cycles to failure at each cyclic stress level (range) for a given material and is specific to the test configuration used in fitting the curve. One must identify appropriate S–N curves for the material based on the *in situ* loading conditions.

To compare the demand and capacity, Miner's rule (Miner, 1945) is used. Expressing Miner's rule (Eq. (2.1.1)) using the notation in this section:

$$C_x = \sum_{k=1}^{K} \frac{n_s(\overline{s}_{xk})}{N(\overline{s}_{xk})} \quad \text{and} \quad C_y = \sum_{k=1}^{K} \frac{n_s(\overline{s}_{yk})}{N(\overline{s}_{yk})} \tag{3.5.1}$$

for the simple SDOF structural models given in Eq. (3.1.1), or

$$C_{xj} = \sum_{k=1}^{K} \frac{n_s(\overline{s}_{xjk})}{N(\overline{s}_{xk})} \quad \text{and} \quad C_{yj} = \sum_{k=1}^{K} \frac{n_s(\overline{s}_{yjk})}{N(\overline{s}_{yk})}, \quad j = 1, \ldots, J \tag{3.5.2}$$

for the linearized FE models given in Eq. (3.1.4). In these equations $N(\cdot)$ represents the number of cycles to failure at the evaluated stress range, which is evaluated from the material's S–N curve. Finally, the damage fractions are combined to evaluate the fatigue damage index (FDI), as follows.

Fatigue Damage Index. The damage fractions C determined from Eq. (3.5.1) or (3.5.2) represent the damage fraction attributed to individual modes (either fundamental only or multiple) in each orthogonal horizontal direction. The value for each damage fraction calculated for the various modes can be combined using the square root of the sum of the squares (SRSS) method, the complete quadratic combination (CQC) method, or an approved equivalent approach. In this study, the SRSS method is assumed in determining the *fatigue damage index* (FDI):

$$\text{FDI} = \sqrt{C_x^2 + C_y^2} \tag{3.5.3}$$

for the simple SDOF structural models given in Eq. (3.1.1), or

$$\text{FDI} = \sqrt{\sum_{j=1}^{J} (C_{xj}^2 + C_{yj}^2)} \tag{3.5.4}$$

for the linearized FE models given in Eq. (3.1.4). The material will fail in fatigue when the FDI equals 1.

3.6 — DISCUSSION

As indicated in Steps 1 (Section 3.1) and 4 (Section 3.4) and Figure 3.1, the mathematical model of the impacted structure is critical in the FDI framework. The mathematical model is used to determine both the fundamental period T which is used to determine the cumulative demand and the stress-displacement relationship from a pushover analysis. Typically, the mathematical model will be in the form of a finite element (FE) model, using software such as SAP2000 (Computers and Structures, Inc., Walnut Creek, CA). If a FE model is not readily available, alternative methods for determining the fundamental period of the bridge include acceptable methods in *AASHTO LRFD Bridge Design Specifications* (AASHTO, 2017), i.e., Eqs. C4.7.4.3.2b-4 or C4.7.4.3.2c-3. Then, an equivalent static seismic load, $p_e(x)$ or p_e, per unit length of bridge would be determined based on either Eqs. C4.7.4.3.2b-5 or C4.7.4.3.2c-4, respectively, where the dimensionless elastic seismic response coefficient, C_{sm}, would be taken as

$$C_{sm} = \frac{1}{g}\left(\frac{2\pi}{T_m}\right)^2 \frac{\overline{D}}{2} \tag{3.6.1}$$

for a given displacement cycle range $\overline{D}$, where g is the acceleration of gravity and T_m is the period of the bridge given by Eqs. C4.7.4.3.2b-4 or C4.7.4.3.2c-3. The equivalent static seismic loading would then be applied to the structure to determine the resulting member stress effects, here denoted s_k.

Steps 2 (Section 3.2) and 3 (Section 3.3) of the FDI procedure are demonstrated in Harvey et al. (2020, Sections 2 and 3, respectively) for two seismic stations in Oklahoma during 2016 considering all M3.0 and larger earthquakes. A similar procedure would be followed for other regions experiencing induced earthquakes.

4 — SUMMARY, CONCLUSIONS, AND RECOMMENDATIONS

Because of the recent increase in seismic activity in the central U.S. caused by human activities (i.e., induced earthquakes), there has been concern raised over the potential for cumulative damaged caused by these frequent, low-level seismic events. The work conducted under this project was aimed at developing a method to quantify the cumulative effect of induced earthquakes on ABC or conventional bridges.

In this ABC-UTC guide, a framework is presented for determining how close a bridge member is to its fatigue life due to repeated seismic loading. The framework comprises five steps, resulting in a quantitative metric for the damage fraction. A metric called the *fatigue damage index* (FDI) is proposed to quantify the percent of a structural element's fatigue life that remains. The FDI is founded on Miner's rule for high-cycle fatigue analysis, incorporating the cumulative seismic demand measures. The framework is demonstrated in the research project Final Report (Harvey et al., 2020) for a "typical" Oklahoma bridge. Additionally, spectral displacement cycle counts are tabulated therein for a range of periods (T = 0.1, 0.2, ..., 0.9, 1, 2, ..., and 10 sec), and traditional intensity measures—spectral acceleration (S_a) and peak ground acceleration (PGA)—are presented for induced earthquakes in Oklahoma during 2016.

The FDI framework is general enough to be applied to other bridges, conventional or ABC, that may be more vulnerable to cumulative damage. The method can be applied for design of new bridges or to evaluate the need for repair/replacement of existing bridges. Future work should consider evaluating accelerated (ABC) solutions for rapid repair/retrofit of (potentially) damaged structures due to induced earthquakes. The viability of accelerated repair solutions for repeated, small-to-moderate earthquakes needs to be assessed. Furthermore, additional verification of the FDI framework is needed; in particular, predictions of fatigue life using the FDI framework should be compared to those found using high-fidelity

FE models, experiments, or a combination thereof.

It is worth mentioning that there is one major limitation of the proposed method: the necessity of a representative S–N curve for the structural element under consideration. The S–N curve needs to be representative of the material and configuration considered. Such curves are usually available for metals (e.g., reinforcing bars, studs, etc.), but for concrete (reinforced or unconfined) are limited. There would be value in maintaining a database of common S–N curves, as well as experimentally determining curves for materials/configurations not presently available. In particular, S–N curves for accelerated repair materials (e.g., ultra-high performance concrete (UHPC)) are needed.

5 — REFERENCES

AASHTO, Guide Specifications for LRFD Seismic Bridge Design, American Association of State Highway and Transportation Officials (AASHTO), Washington D.C., 2009.

AASHTO, AASHTO LRFD Bridge Design Specifications, American Association of State Highway and Transportation Officials (AASHTO), Washington, D.C., 8th edition edn., 2017.

ASTM E1049-85(2017), Standard Practices for Cycle Counting in Fatigue Analysis, ASTM International, 2017.

Beyer, K., Bommer, J. J., Relationships between median values and between aleatory variabilities for different definitions of the horizontal component of motion, *Bulletin of the Seismological Society of America* 96 (2006) 1512–1522, doi:10.1785/0120050210.

Boore, D., Watson-Lamprey, J., Abrahamson, N., Orientation-Independent Measures of Ground Motion, *Bulletin of the Seismological Society of America* 96 (4A) (2006) 1502–1511, doi:10.1785/0120050209.

Chase, R. E., Liel, A. B., Luco, N., Baird, B. W., Seismic loss and damage in light-frame wood buildings from sequences of induced earthquakes, *Earthquake Engineering & Structural Dynamics* 48 (12) (2019) 1365–1383, doi:10.1002/eqe.3189.

Chopra, A. K., Dynamics of Structures: Theory and Applications to Earthquake Engineering, Prentice Hall, Englewood Cliffs, New Jersey, 5th edn., 2017.

Culmo, M. P., Accelerated bridge construction-experience in design, fabrication and erection of prefabricated bridge elements and systems, Tech. Rep. FHWA-HIF-12-013, Federal Highway Administration, Washington, DC, 2011.

Frankel, A. D., Applegate, D., Tuttle, M. P., Williams, R. A., Earthquake hazard in the New Madrid Seismic Zone remains a concern, U.S. Geological Survey Fact Sheet: 2009-3071, 2 p, 2009.

Harvey, Jr., P. S., Heinrich, S. K., Muraleetharan, K. K., A Framework for Post-Earthquake Response Planning in Emerging Seismic Regions: An Oklahoma Case Study, *Earthquake Spectra* 34 (2) (2018a) 503–525, doi:10.1193/053117EQS100M.

Harvey, Jr., P. S., Kaid Bay Cortez, I. A., Heinrich, S. K., Response of a Typical Oklahoma Bridge to the September 3, 2016, 5.8-Magnitude Earthquake near Pawnee, Oklahoma, *Journal of Bridge Engineering* 23 (2) (2018b) 04017130, doi:10.1061/(ASCE)BE.1943-5592.0001178.

Harvey, Jr, P. S., Muraleetharan, K. K., Sivakumaran, S., Rapid Retrofitting Techniques for Induced Earthquakes, Final Report ABC-UTC-2016-C1-OU02-Final, Accelerated Bridge Construction University Transportation Center (ABC-UTC), available at http://www.abc-utc.fiu.edu, 2020.

Keranen, K. M., Savage, H. M., Abers, G. A., Cochran, E. S., Potentially induced earthquakes in Oklahoma, USA: Links between wastewater injection and the 2011 Mw 5.7 earthquake, *Geology* 41 (6) (2013) 699–702, doi:10.1130/G34045.1.

Matsuishi, M., Endo, T., Fatigue of Metals Subjected to Varying Stress, in: Japan Society of Mechanical Engineers, 1968.

McGarr, A., Bekins, B., Burkardt, N., Dewey, J., P. Earle, W. E., Ge, S., Hickman, S., Holland, A., E. Majer, J. R., Sheehan, A., Coping with earthquakes induced by fluid injection, *Science* 347 (6224) (2015) 830–831, doi:10.1126/science.aaa0494.

Miner, M. A., Cumulative Fatigue Damage, *Journal of Applied Mechanics* 12 (1945) A159–A164.

Petersen, M., Moschetti, M., Powers, P., Mueller, C., Haller, K., Frankel, A., Zeng, Y., Rezaeian, S., Harmsen, S., Boyd, O., Field, N., Chen, R., Rukstales, K., Luco, N., Wheeler, R., Williams, R., Olsen, A., Documentation for the 2014 update of the United States national seismic hazard maps, Tech. Rep. Open-File Report 2014-1091, U. S. Geological Survey, doi:10.3133/ofr20141091, 2014.

Petersen, M. D., Mueller, C. S., Moschetti, M. P., Hoover, S. M., Llenos, A. L., Ellsworth, W. L., Michael, A. J., Rubinstein, J. L., McGarr, A. F., Rukstales, K. S., 2016 One-Year Seismic Hazard Forecast for the Central and Eastern United States from Induced and Natural Earthquakes, Open-File Report 2016-1035, U.S. Geological Survey, Reston, Virginia, doi:10.3133/ofr20161035, 2016.

USGS, Induced Earthquakes, *Earthquake Hazards Program*, U. S. Geological Survey, URL https://earthquake.usgs.gov/research/induced/overview.php, accessed February 17, 2017, 2017.

ABC UTC

ACCELERATED BRIDGE CONSTRUCTION
UNIVERSITY TRANSPORTATION CENTER

IOWA STATE UNIVERSITY

University of Nevada, Reno

FIU
Civil and Environmental Engineering

WASHINGTON

The UNIVERSITY of OKLAHOMA